NEUROSCIENCE
RESEARCH ARTICLE

P. C. Patta et al. / Neuroscience 497 (2022) 271–281

# Nanoscale Structural Characterization and Impact on Long-term memory of Amyloid-β42 Oligomeric forms in Zebrafish

**Paulo C. Patta,** [a†‡] **Elisa M. N. de Oliveira,** [b†¶] **Ana Carolina F. Goulart,** [a,b‖] **Amanda B. Zaluski,** [a|] **Ricardo M. Papaléo** [b§] **and Monica R. M. Vianna** [a*††]

[a] *Laboratório de Biologia e Desenvolvimento do Sistema Nervoso, Escola de Ciências da Saúde e da Vida, Pontifícia Universidade Católica do Rio Grande do Sul, Porto Alegre, RS, Brazil*

[b] *Centro Interdisciplinar de Nanociências e Micro-Nanotecnologia, Escola Politécnica, Pontifícia Universidade Católica do Rio Grande do Sul, Porto Alegre, RS, Brazil*

**Abstract—The contribution of amyloid-β (Aβ) soluble forms to Alzheimer's Disease (AD) is undergoing revision and the characterization of monomeric, oligomeric and protofibrillar Aβ forms used *in vivo* to model AD is a critical step to ensure data interpretation. Atomic force microscopy (AFM) was used to characterize the nanoscale morphology of different $A\beta_{42}$ forms also used for cerebroventricular injection (cvi) in young (6mo) and aged (36mo) adult zebrafish behavioral and cognitive tests. On the AFM, monomeric solution deposited onto mica resulted mostly in thin filamentous structures and shorter monomeric agglomerates with heights around or below 1.5 nm, as expected for single $A\beta_{42}$. The oligomeric form was dominated by particles with globular morphology and a few short aggregates around 1 nm high and 8–12 nm long. The protofibrillar form had micrometer-long twisted fibrils of varying diameters (4.5–10 nm) and large entangled clusters with sizes of up to several tens of micrometers. On the Open Tank used to test exploratory parameters, no differences were observed between injected animals and their age-matched controls, except for a reduced distance travelled by aged individuals that received the $A\beta_{42}$ oligomeric form. Long-term memory (LTM) for the inhibitory avoidance task was not influenced by monomers cvi, whilst oligomeric and fibrillar $A\beta_{42}$ hindered LTM formation in young and aged groups. Our findings support current views of deleterious effects of $A\beta_{42}$ soluble forms on cognition and ensures that preparations were structurally unique and within expected morphologies and dimensions.**

***This article is part of a Special Issue entitled: In memory of Ivan Izquierdo South American pioneer of the Neuroscience of Memory Temporal dynamics and molecular mechanisms.*** 

**Key words: $A\beta_{42}$ oligomeric states, zebrafish, long-term memory, AFM.**

## INTRODUCTION

Alzheimer's disease (AD) affects an estimate of 50 million people worldwide and lacks effective treatments, with most phase III drug clinical trials failing to significantly impact the disease progression (Schneider et al., 2015; Livingston et al., 2017; Kametani and Hasegawa, 2018; International Alzheimer's Disease, 2019). As the most prevalent form of dementia, mostly associated with aging, AD is projected to increase its social and economic burden in the next decades, especially in less developed countries. The AD hallmarks include extracellular senile plaques composed mainly by amyloid-β (Aβ) peptides varying in length mainly from 39 to 43 amino acids (aa), produced by the sequential cleavage of the amyloid precursor protein (APP) by β and γ secretases (Chen and Tang, 2006; Li et al., 2018). Monomeric Aβ peptides tend to associate into oligomer intermediates of varied sizes and to progress to larger supramolecular structures such as fibrils and plaques (Hortschansky et al., 2005; Cohen et al., 2013). While the 40 aa ($A\beta_{40}$) size is the most abundant in the brain, the 42 aa ($A\beta_{42}$), less soluble and more aggregation prone, actively induces fibril formation and Aβ accumulation (Hortschansky et al., 2005). In aged indi-

*Corresponding author.
E-mail addresses: paulo.patta90@edu.pucrs.br (P. C. Patta), elisa.oliveira@acad.pucrs.br (E. M. N. de Oliveira), ana.goulart@edu.pucrs (A. C. F. Goulart), amanda.zaluski@edu.pucrs.br (A. B. Zaluski), papaleo@pucrs.br (R. M. Papaléo), monica.vianna@pucrs.br (M. R. M. Vianna).
† Both authors contributed equally.
‡ ORCID: 0000-0002-9734-6950.
¶ ORCID: 0000-0003-2623-8589.
‖ ORCID: 0000-0002-7464-5069.
| ORCID: 000-0003-1638-5331.
§ ORCID: 0000-0003-3726-8951.
†† ORCID: 0000-0002-1881-127X.

*Abbreviations:* ACH, amyloid-β cascade hypothesis; AD, Alzheimer's disease; AFM, atomic force microscopy; AOH, amyloid-β oligomer hypothesis; APP, amyloid precursor protein; Aβ, beta amyloid peptide; $A\beta_{40}$, amyloid $\beta_{40}$; $A\beta_{42}$, amyloid $\beta_{42}$; CV, cerebroventricular injections; DMSO, dymethilsufoxide; EtOH, ethanol; Veh, vehicle solution.

https://doi.org/10.1016/j.neuroscience.2022.02.031
0306-4522/

viduals and AD patients, the increased levels of $A\beta_{42}$ accelerate the formation of larger aggregates (Kametani and Hasegawa, 2018).

The Amyloid Cascade Hypothesis (ACH) (Hardy and Higgins, 1992) originally postulated that the Aβ aberrant peptide initiates a series of damaging events when it accumulates in the brain, pointing to insoluble plaques as the disease culprit. The ACH has been updated as evidence accumulates demonstrating that the Aβ burden does not correlate with AD progression (Josephs et al., 2009; Sakono and Zako, 2010; Li et al., 2018). Soluble Aβ oligomeric forms, intermediary to monomers and insoluble plaques, are the most active agents of neurotoxicity and synaptic dysfunction (Demuro et al., 2005; Sakono and Zako, 2010; Tu et al., 2014; Washington et al., 2014; Kametani and Hasegawa, 2018), and the Amyloid-β Oligomer Hypothesis (AOH) (reviewed in (Cline et al., 2018)), that support their role as the most pathological forms, has gained strength (Sakono and Zako, 2010; Benilova et al., 2012). The monomeric Aβ, in turn, has been attributed new roles and suggested to be a constitutive peptide in human physiology, as extensively reviewed in (Brothers et al., 2018; Moir et al., 2018). These new perspectives press to a better understanding of Aβ and its different oligomeric states in AD and other physiological contexts.

Understanding AD progression and its cellular and molecular mechanisms depends on animal models to emulate the disease conditions. Transgenic and knockout mice studies brought many insights to Aβ metabolism and genetics (Heber et al., 2000; Luo et al., 2003; Cortes-Penfield et al., 2016). Cerebroventricular (CV) injection of $A\beta_{42}$ is a useful as a strategy to study the effects of the peptide quaternary forms and the *in vivo* aggregation in animal models, including rodents (Shankar et al., 2008) and marmoset monkeys (Ridley et al., 2006). Zebrafish shares 84% of human genes related to diseases (Howe et al., 2013), has homologs to all the characterized AD substrates and has also been used to study, AD by the generation of mutants (Pu et al., 2016), morpholinos (Nery et al., 2017; Stainier et al., 2017) or combinations between these and other approaches (Newman et al., 2014; Saleem and Kannan, 2018). The effects of $A\beta_{42}$ CV injection were previously studied in adults (Bhattarai et al., 2017a; Thomas et al., 2017; Javed et al., 2019) and larvae, in which we demonstrated that oligomeric forms induced cognitive impairment and increased tau phosphorylation, other AD hallmarks (Nery et al., 2014). Nevertheless, the effects of the different oligomeric states of $A\beta_{42}$ were not compared on previous studies, nor combined with other associated disease factors such as age.

The characterization of different Aβ preparations used *in vivo* to model AD is a critical step to ensure data interpretation. Nanotechnology can contribute to the elucidation of molecular mechanisms of AD (Nazem and Mansoori, 2008) and atomic force microscopy (AFM) can be used to capture structural images and measure the mechanical nanoscale properties of Aβ in different oligomeric states using specific conditions, substrates and solvents (Adamcik et al., 2010; Adamcik and Mezzenga, 2012; Enache et al., 2016; Lin et al., 2019; Watanabe-Nakayama et al., 2020). Studies using AFM to characterize Aβ structure, however, used unique conditions and did not compare multiple oligomeric forms nor paralleled their findings to *in vivo* analysis of its effect.

Here we characterize solutions enriched of human $A\beta_{42}$ peptide prepared to be in monomeric, oligomeric, and protofibrillar states using AFM and describe their cognitive effects after CV injection in young and aged adult zebrafish. This may contribute to future studies aiming to use these preparations and serves as a model to further dissect the physiological and behavioral effects of different $A\beta_{42}$ conformations in aging individuals.

## EXPERIMENTAL PROCEDURES

This study was conducted at the Laboratório de Biologia e Desenvolvimento do Sistema Nervoso of the School of Health and Life Sciences and at the Interdisciplinary Center of Nanoscience and Micro-Nanotechnology (Nano-PUCRS) of the School of Technology at the Pontificia Universidade Catolica do Rio Grande do Sul (PUCRS). Animals were housed at the Center for Experimental Biological Models (CeMBE-PUCRS). Protocols were approved by the Scientific Committee from the School of Health and Life Sciences and by the Institutional Animal Care Committee (CEUA-PUCRS, permit number 15/00485) and followed the Guidelines of the to the Brazilian National Council for the Control of Animal Experimentation (CONCEA), (MCTIC (Ministério da Ciência, Tecnologia, 2016).

### Experimental design

$A\beta_{42}$ in different aggregation states (monomeric, oligomeric, and protofibrillar) were freshly prepared, as detailed in the next section, to be used within the schedule depicted in Fig. 1, avoiding unnecessary manipulation and heating. The same solutions were used for CV injection and AFM structural characterization.

Young and aged adults were assigned to the following groups according to the solutions received by CV injection: Controls received the $A\beta_{42}$ solution vehicle (veh), which was 0.25% dymethilsufoxide (DMSO) in water, while $A\beta_{42}$ 10 μM solutions were diluted from 1 mM solutions (described in detail in 2.2) prepared to be enriched in Monomers ($A\beta_{42}$M), Oligomers ($A\beta_{42}$O) and Protofibrils ($A\beta_{42}$P). To each experimental group, at both ages, the CV injection was performed in approximately 15 seconds and fishes were returned to tank for recovery. All injections were performed on the same day. Animals were routinely inspected for abnormal behavior for the following 22 days. At 7 days post injection (dpi), the open tank test was performed to evaluate general exploratory capacity. At 21 dpi, animals were tested for long-term aversive memory on the inhibitory avoidance task. The experimental approach was designed to answer our scientific questions, avoiding interference from one behavioral manipulation on the following.

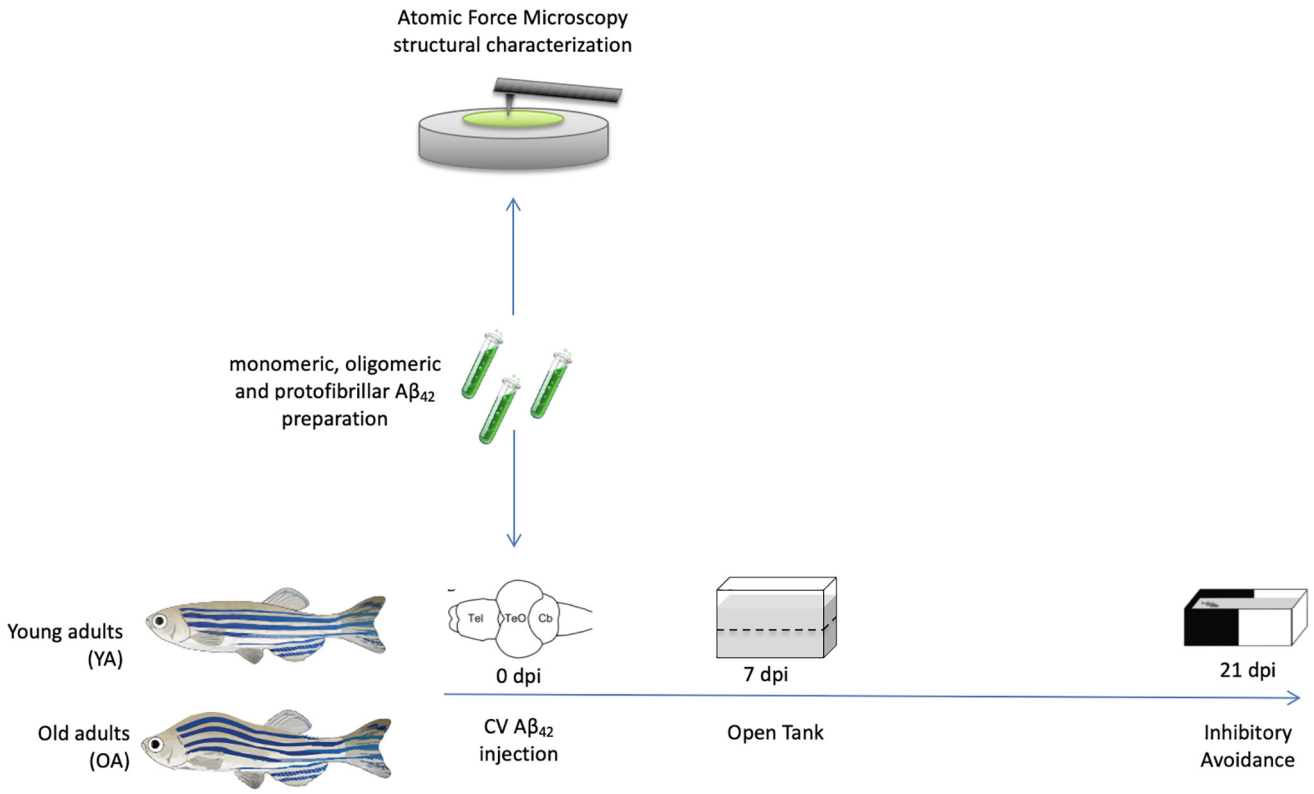


**Fig. 1.** Experimental design.

After the preparation of $A\beta_{42}$ in different oligomeric states, solutions were structurally characterized using AFM and used for CV injection in young and aged adults. Seven dpi, animals were exposed to the open tank test for 5 minutes to access their exploratory behavior. They were daily monitored until the inhibitory avoidance training and test sessions, performed at 21 and 22 dpi, respectively, to evaluate animals' long-term memory.

### Preparation of different $A\beta_{42}$ forms

The $A\beta_{42}$ peptide (Sigma-Aldrich – A9810) was prepared according to the adapted protocol from (Cunvong et al., 2013) as described by (Nery et al., 2014). Briefly, the peptide was first dissolved in DMSO 100% and then diluted in ultrapure water to a stock concentration of 1 mM $A\beta_{42}$. To produce the monomeric form, the stock solution was diluted to 10 μM (0.25% DMSO) and stored at −20 °C to prevent $A\beta_{42}$ unwanted aggregation. To prepare a solution composed mainly by oligomers, a fraction of the monomeric solution was incubated for 5 days at 37 °C, as described by Cameron et al. (Cameron et al., 2012). After, the oligomer solution was frozen in liquid nitrogen and stored at –20 °C. To prepare the protofibril-enriched solution, a fraction of the monomeric preparation was also incubated on a shaker (800 rpm), at 23 °C for 36 hours, and then centrifuged (10 min × 15,000*g*), frozen in liquid nitrogen, and stored at –20 °C (O'Hare et al., 1999). It is known that freshly prepared monomeric Aβ42 readily aggregates into soluble oligomers in a concentration and temperature dependent mode (Sakono and Zako, 2010; Cameron et al., 2012; Novo et al., 2018), so it was imperative to prepare the solutions with utmost care.

### Characterization of the $A\beta_{42}$ oligomeric preparations using atomic force microscopy

Morphological analyses of all $A\beta_{42}$ preparations described above were performed by Atomic Force microscopy (AFM – Bruker, model Dimension Icon), operating in the Peak Force Tapping and Peak Force QNM modes. Prior to imaging, an aliquot (50 μL) of each $A\beta_{42}$ form was deposited onto freshly cleaved mica surfaces and dried under ambient conditions. Images were acquired with Bruker's ultrasharp Scanasyst Air Si tips on silicon nitride cantilevers (tip nominal radius of 2 nm), with spring constant of 0.4 N/m and resonant frequency of 70 kHz. Peak force frequency was typically around 2 kHz and peak force amplitude varied between 50–100 nm. Samples were probed at different scanning sizes (from 500 nm to 50 μm), with 256-or 512 lines/image and scanning rates of either 0.50 or 1 Hz/line. Image analysis was performed using the manufacturer's software (Nanoscope, Bruker) and Image J.

### Animals and maintenance

Young (6 months, 0.4–0.6 g) and aged (36 months, 0.8–1.2 g) wild-type AB zebrafish (*Danio rerio*) were maintained in an automated recirculating multilink tank system (Zebtec, Tecniplast, Italy) at a density of 1.5 fish per liter with conditioned reverse osmosis-filtered water

to keep the species standard parameters of conductivity, temperature (28 °C ± 2 °C), pH (7.5), ammonia, nitrite, nitrate, and chlorine levels. Animals were subjected to a light/dark cycle of 14/10 h and fed commercial flakes (TetraMin Tropical Flake Fish®) three times a day supplemented with live brine shrimp (*Artemia salina*) (Westerfield, 2007). Male and female individuals were used irrespective of their gender. Fish from each experimental group were randomly chosen for behavioral tests and transferred from the growing tanks to glass tanks (13 × 30 × 18 cm) in which they were kept during behavioral analyses. Glass tank maintenance included a 2/3 water change three times a week after removal of the excess of food or fish waste from the bottom using a siphon and kept the same water quality parameters and fish density.

### Cerebroventricular injection

To deliver the $A\beta_{42}$ to the brain, a protocol of cerebroventricular (CV) injection was adapted from previous studies (Bhattarai et al., 2017b; Javed et al., 2019). Briefly, fish were anesthetized in Tricaine MS-222 (100 mg/L, 0.01% in water) and placed on a wet slitted sponge. They were gently held while CV injection was performed using a 1 μL Hamilton glass syringe. The $A\beta_{42}$ monomeric ($A\beta_{42}$ M), oligomeric ($A\beta_{42}O$), and protofibrillar ($A\beta_{42}P$) solutions (1 μL, 10 μM final concentration) were injected between the right and left telencephalon lobes.The needle did not enter more than 1 mm. The syringe was washed twice with 70% EtOH and 1× PBS after every injection. After injection, which lasted no more than 30 seconds for each individual, animals were placed back on their original tanks to recover. After around 10 minutes, their movement and breathing were visually normalized. Around 3% of animals, irrespective of their experimental groups, have shown aberrant swimming behavior in the first 24 h and were euthanized. The remaining injected animals were daily checked for the remaining 22 days of experimentation and no sign of abnormal behavior were observed.

### Open tank test

The open tank test was used to evaluate animals swimming parameters 7 days after the injection (dpi) (Wong et al., 2010). Animals were placed individually in experimental tanks (30 cm long × 15 cm high × 10 cm wide) and were recorded for 6 min. Locomotion and exploratory patterns of each fish were analyzed after the first minute of habituation using EthoVision XT software (Version 11.5, Noldus) at a rate of 30 positions per second (Altenhofen et al., 2017). Each group had $n = 20$. Normality and lognormality of data were analyzed by Kolmogorov–Smirnov. The following behavioral parameters were parametric and analyzed by ANOVA followed by Tuckey's test of multiple comparisons: distance traveled (m), mean speed of mobile time (m/s) and percentile of mobile time (%). Statistical analyses of behavioral tests were performed using Graphpad Prism 8 software (GraphPad Software, San Diego, CA, USA). In all statistical analysis, the level of significance was set as $p < 0.05$.

### Inhibitory avoidance test

To ascertain if the different $A\beta_{42}$ solutions caused long-term memory deficit, an inhibitory avoidance task was performed as established by Blank et al. (Blank et al., 2009). From twenty-one dpi, animals were submitted to training and test sessions separated by 24 h at the inhibitory avoidance apparatus, a glass tank (18 cm length × 9 cm width × 7 cm height) with two equally sized compartments divided by a sliding glass guillotine-type partition (9 cm × 7 cm). Compartments were defined by opaque plastic self-adhesive films in black or white colors externally covering all surfaces of the corresponding sides (Fig. 1). Two electrodes extending through the wall height and placed on each far side of the opposing walls of the dark compartment were attached to an 8 V stimulator and administered a final 3 ± 0.2 V AC shock (intensity measured between electrodes and the center of the dark compartment) when manually activated. Animals were gently placed in the white side of the task tank while the partition between compartments was closed. After 1 min of habituation, the partition was raised 1 cm, allowing fish to cross to the dark side of the tank.

On the training session, when animals entered to the dark side with their entire body, the sliding partition was closed, and a pulsed electric shock was administered for 5 s. After this session, the fish was removed from the apparatus and placed in a temporary housing tank until all animals were tested, when all were returned to their original tank. Animals were tested for long-term memory retention 24 h after training. The test session repeated the training protocol, except that the shock was not administered and immediately after animals crossed to the dark compartment, they were removed from the apparatus. The latencies to cross from the white to the dark side were recorded in both sessions. While no ceiling time was used at the training learning session to unbiasedly evaluate the possible effects of age and treatment, during testing the maximum time animals were allowed to spend in the white compartment was 180 s (ceiling time). If that happened, animals were gently removed and their latency was considered to be 180 s. This ensured all behavioral experiments were caried out in the mornings and were less impacted by circadian fluctuations in activity and feeding schedule. Each group had 8–12 individuals. After the test, animals were euthanized by hypothermal shock (Matthews and Varga, 2012).

Normality and lognormality of data were analyzed by Kolmogorov–Smirnov. Data for inhibitory avoidance were non-parametric and evaluated accordingly. Training and test sessions were compared between age-matched groups by Kruskal–Wallis. Long-term memory retention was estimated by comparing training and test session latencies within each group by Mann-Whitney. Statistical analyses of behavioral tests were performed using Graphpad Prism 8 software (GraphPad

Software, San Diego, CA, USA). In all statistical analysis, the level of significance was set as $p < 0.05$.

## RESULTS

### $A\beta_{42}$ structural characterization

AFM was employed to identify the predominant nanoscale morphology of amyloid structures in the different forms prepared from aqueous solutions. Fig. 2 summarizes the main findings. The monomeric solution deposited onto mica resulted mostly in thin filamentous structures together with a distribution of shorter monomeric agglomerates as can be seen in Fig. 2A–F. Fig. 2B shows a zoom on a filament cluster. Sections across a series of filaments (dashed line *L* in Fig. 2B) and along a selected filament F1 show heights around or below 1.5 nm (Fig. 2C, D). The full height distribution of such filaments and shorter particles lies between 0.5–1.2 nm (second peak in Fig. 2e), which is very close to the expected radius of gyration of $A\beta_{42}$ monomers derived from mobility studies and MD simulations (Baumketner, 2006) and from height distributions previously reported for monomeric $A\beta_{42}$ (Banerjee et al., 2017). In our analysis, the most frequent structures seen on mica have a wire shape, with length varying from 30-200 nm (Fig. 2E). The profile along the length of filament F1 in Fig. 2D shows repeated height variations with a periodicity of about 5 nm, suggesting that they are formed from a linear array of monomers. Considering the great tendency of $A\beta_{42}$ to aggregate and the ordering effect of electrostatic interactions on the mica surfaces (Giacomelli and Norde, 2005; Moores et al., 2011), we hypothesize that the 1 nm-high filaments are mainly formed during the process of drying after deposition. Indeed, when a higher monomer concentration is used in the solutions, the deposition results in a continuous monolayer film of $A\beta_{42}$.

Interestingly, in the deposits of the oligomer-enriched preparation (Fig. 2G–K) such thin filament structures are rare. Structures observed on the mica surface are dominated by particles with globular morphology (usually identified as oligomers with various repetition units (Dahlgren et al., 2002a; Banerjee et al., 2017) and a few short elongated aggregates. In the magnified view of Fig. 2H, the arrows highlight the two most common structures labelled as O1 and O2. Sections across these features are depicted in Fig. 2I. The type O1 has a mean height close to 1 nm and maximum length between 8–12 nm. O2 has typically heights around 1.5–2 nm and lengths between 16–20 nm. Height and length distributions obtained from section analysis of about 100 particles are given in Fig. 2J,K, respectively. Clearly, oligomers have much less tendency to aggregate in chains (at least on mica surfaces) than monomers and the vast majority of structures seen on the AFM images have lateral extent below 20 nm. The globular morphology was also observed elsewhere as transient forms on the pathway of fibril formation (Dahlgren et al., 2002a; Glabe, 2008).

The deposits from the protofibrillar preparation, on the other hand, are dominated by micrometer-long twisted fibrils (Fig. 2L, N) and large entangled fibril clusters with sizes of up to several tens of micrometers. The morphology and diameter of such fibers is distinctively different from the structures seen on the monomer and oligomer preparations. Height distributions taken on a fibril cluster (Fig. 2Q) show a predominance of heights (i.e., fibril diameters) around 4–5 nm (as the fibril labeled T2 in Fig. 2I and seen in the magnified image in Fig. 2N), but a fraction has diameters close to 10 nm (T4, Fig. 2L, P) or more. Fibril length is broadly distributed (Fig. 2R) and the average value obtained in 5 μm AFM scans is 2.5 ± 1.3 μm. The predominant twisted fibril type with diameters around 4 nm has a pitch length deduced from height profiles (Fig. 2P) around 34–36 nm. These characteristics are consistent with the fibrils being composed of two twisted protofilaments, about 2 nm each, as indicated by coarse-grain molecular dynamics simulations and confirmed by AFM imaging (Adamcik et al., 2010; Adamcik and Mezzenga, 2012). The fibrils may have varying diameters along their length and rounded junctions at the point of intersection of several units. Thicker fibrils show a larger pitch, sometimes close to 100 nm, compatible with twisted ribbons composed of four protofilaments (Adamcik and Mezzenga, 2012). Such structures are, nevertheless, rare. Also visible in the AFM images are bundles of ~1 nm-high filaments (marked as FB in Fig. 2L, M), similar to those found on images from the monomeric deposits. These filaments are better contrasted in adhesion images (Fig. 2M, O). A close inspection of the regions around fibrils (Fig. 2O) shows that many of them lie close or on top of such narrow filament structures.

### Behavioral and cognitive effects in young and aged adults

Zebrafish has been reported to live up to 4 years in captivity and old individuals are generally considered to have more than 2 years (Yu et al., 2006; Gilbert et al., 2013; Parichy, 2015). They grow continuously over time and is well established that zebrafish body size is significantly impacted by breeding and maintenance conditions and at younger ages a significant variation in size is observed between individuals of the same developmental age (Singleman and Holtzman, 2014). As expected, young animals were smaller than aged ones, but within expected sizes for the species. Individuals from our aged group were 3 years old and showed phenotypic signs of aging, as the typical spinal curvature (Hayes et al., 2013), but remained active and social among their shoal mates. Considering the dimensions of our behavioral apparatus, no significant effect of their body size is expected to influence our findings.

### Open tank

After 7 dpi, animals were submitted to the Open Tank Test to access the following exploratory and locomotory parameters: distance travelled (m), mean speed (m/s), and mobile time (%). No differences were observed between young adults' groups in mean speed (Fig. 3A), distance travelled (Fig. 3B), and mobile time (Fig. 3C).

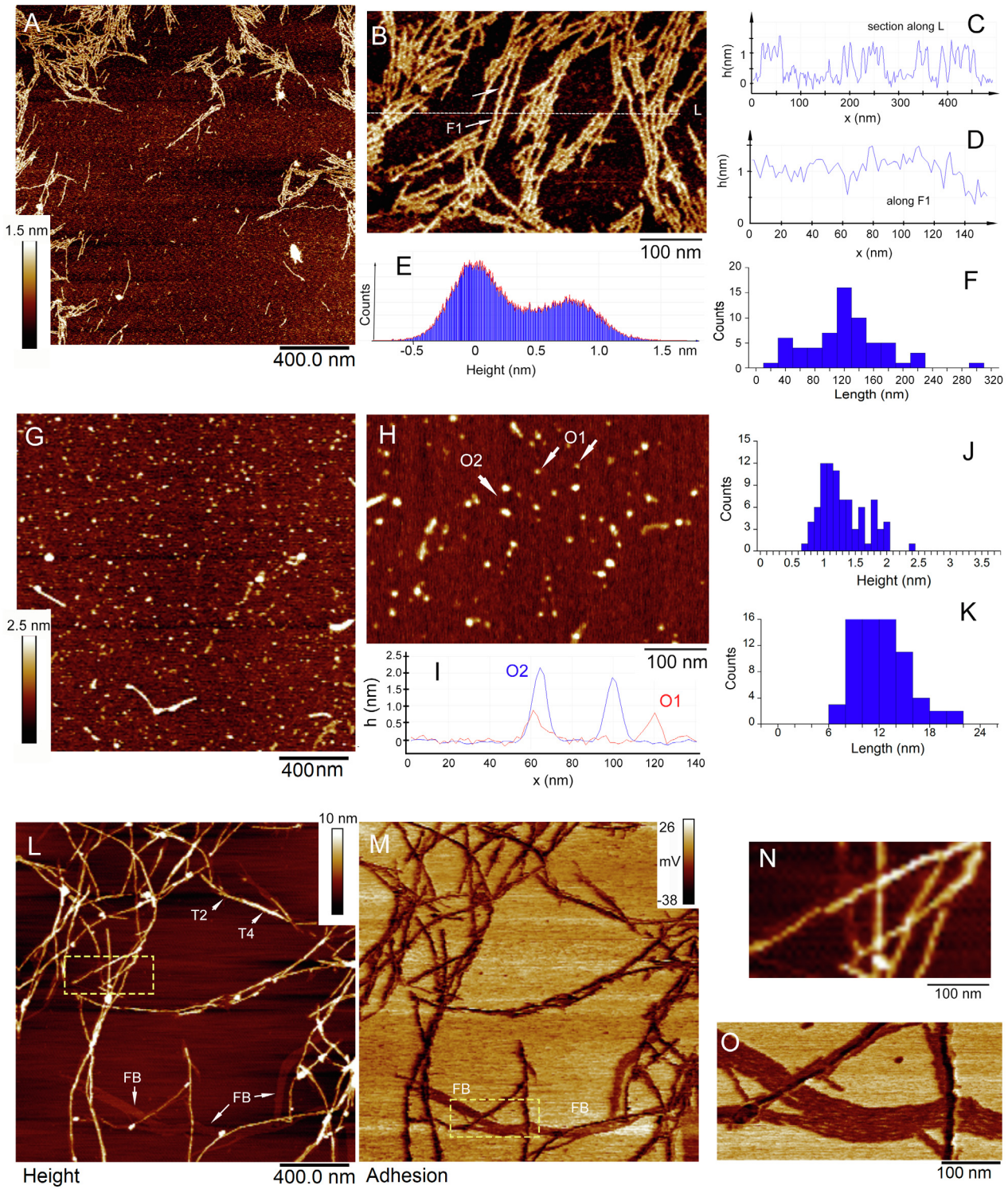
A
1.5 nm
400.0 nm
B
F1
L
100 nm
C
section along L
h(nm)
x (nm)
D
along F1
h(nm)
x (nm)
E
Counts
Height (nm)
F
Counts
Length (nm)
G
2.5 nm
400nm
H
O1
O2
100 nm
I
O2
O1
h (nm)
x (nm)
J
Counts
Height (nm)
K
Counts
Length (nm)
L
10 nm
T2
T4
FB
FB
Height
400.0 nm
M
26
mV
-38
FB
FB
Adhesion
N
100 nm
O
100 nm
P
along T2
across T4
T2
h (nm)
x (nm)
Q
Counts
Height (nm)
R
Counts
Length (nm)

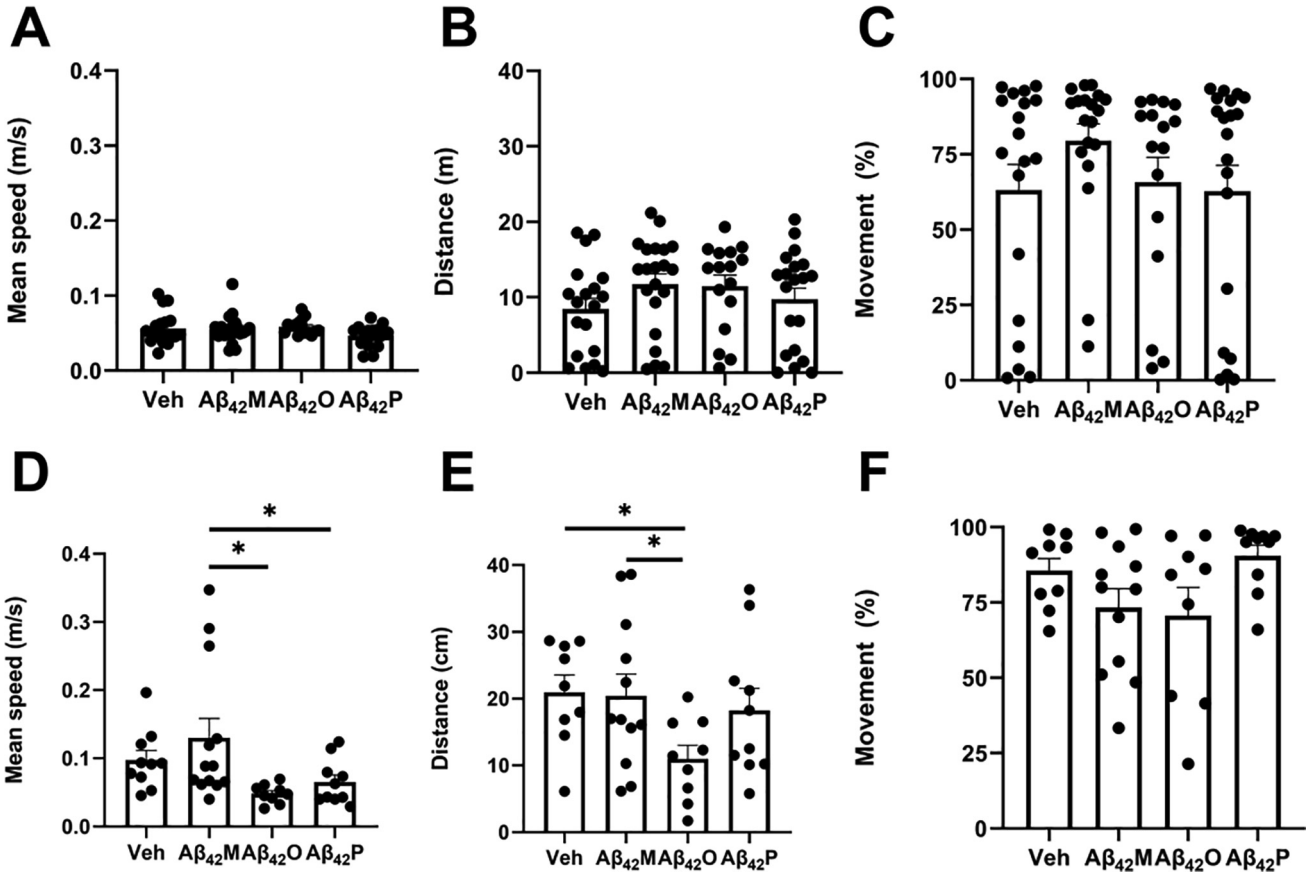


**Fig. 3.** Open Tank Test. Mean speed of mobile time (m/s) of young **(A)** and aged animals **(D)**, Distance travelled (cm) of young **(B)** and aged animals **(E)** and time in movement (%) of young **(C)** and aged animals **(F)** during a 5-minute session. Mean speed, Distance travelled, and Movement were analyzed by One-way ANOVA, followed by Tukey test. For all graphics, values are presented as Mean ± SEM and $n = 20$. Dots represent individual values. Asterisks express differences between groups indicated by the line at $p < 0.05$.

Mean speed (Fig. 3D), despite no significant differences between aged $A\beta_{42}$ groups and their age-matched control, was reduced when $A\beta_{42}M$ and $A\beta_{42}O$ ($p = 0.0124$) and $A\beta_{42}M$ and $A\beta_{42}P$ ($p = 0.0468$) were compared. The total distance travelled (Fig. 2E) also differed between Veh and $A\beta_{42}O$ ($p = 0.0468$) and $A\beta_{42}M$ and $A\beta_{42}O$ ($p = 0.0443$). No significant changes in mobile time were observed between aged individuals (Fig. 3F). Additionally, when we analyze the overall exploratory pattern of young and aged controls, aged controls are faster and therefore explore longer distances in the 5 min session than younger controls, which could be attributed to their larger size.

### Inhibitory avoidance

We then asked if $A\beta_{42}$ injection would elicit long-term memory deficits in young and aged animals after 21 dpi. First, we analyzed overall performance to ensure training sessions of animals from all groups and ages were not different, suggestive of equivalent learning capacities, as supported by the exploratory parameters from the Open tank Test (Fig. 3). Training session latencies from vehicle-injected control groups of both ages were also equivalent. Memory retention, represented by the significant increase in latencies from training to test sessions, was evident in young adult Veh

**Fig. 2.** AFM analysis of the monomer **(A–F)**, oligomer **(G–K),** and protofibril preparations **(I–R)** deposited onto mica surfaces. **(A)** AFM topographical image of monomeric solutions dried on a mica surface. **(B)** Magnified view on a filament cluster. **(C)** Cross-section along several filaments along the dashed line L marked in **(B)**. **(D)** Longitudinal section along filament F1 shown in **(B)**. **(E)** Height and **(F)** length distributions of particles seen on AFM images. In **(E)** the peak centered at zero correspond to pixels at the surface level and the second distribution centered at 0.8 nm to the height of particles. **(G)** AFM image of the oligomer preparation. **(H)** Magnified view, highlighting the two most common oligomer types (labeled O2 and O1). Cross sections over those particles are given in **(I)**. **(J)** Height and **(K)** length distributions of oligomers (excluding rare extended agglomerates seen in **(G)**. **(L)** AFM height and **(M)** adhesion images of fibrilar preparations dried on mica. The yellow boxes indicate regions zoomed in **(N)** and **(O)**. T2 and T4 mark the most frequent fibrillar structures found in the images, whose profiles are given in **(P)**. FB are thin filament bundles, similar to filaments that appear in the monomer deposits. **(Q)** Height and **(R)** length distribution of the fibrils.

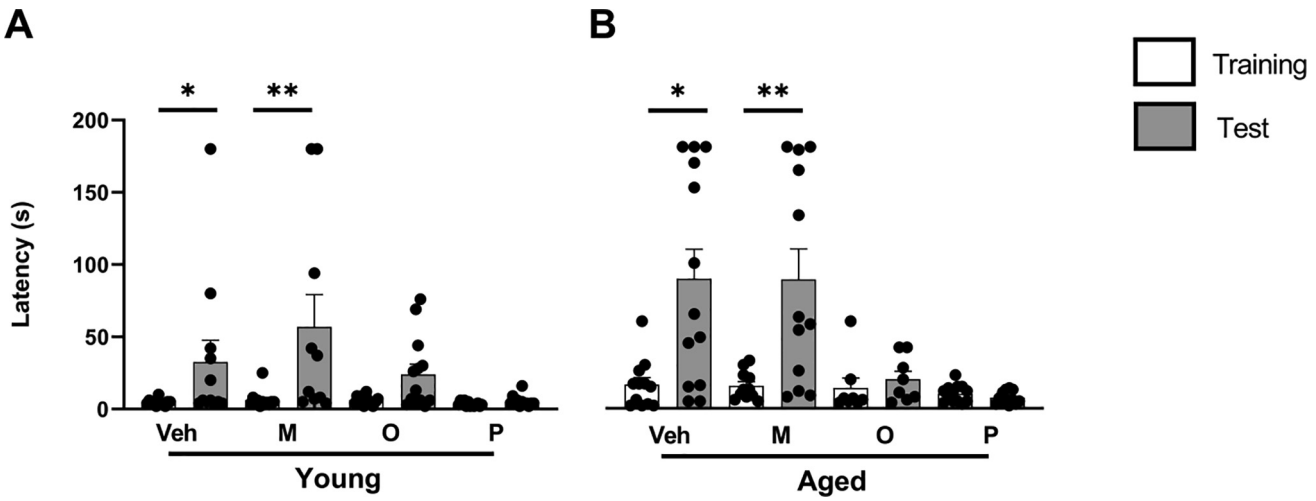


**Fig. 4.** Inhibitory avoidance. Columns show mean latencies (s) + SEM to cross from white to dark compartment in training (clear) and test (shaded) sessions for **(A)** young and **(B)** aged animals ($n$ = 8–12). **(A)** Represents the young groups and **(B)** the aged groups. No differences were found between training performances among all groups when compared by Kruskal–Wallis test. Asterisks express within group differences from training and test sessions by Mann-Whitney ($n$ = 8–12; * $p < 0.05$; ** $p < 0.01$).

and $A\beta_{42}M$ ($p$ = 0.0343 and 0.0033, respectively), while $A\beta_{42}O$ and $A\beta_{42}P$ did not show long-term memory retention (Fig. 4A). Similar results were observed for aged zebrafish: only $A\beta_{42}$ Veh and $A\beta_{42}M$ showed retention ($p$ = 0.0082 and 0.0082, respectively) while $A\beta_{42}O$ and $A\beta_{42}P$ were not (Fig. 4B). Overall, despite the lack of statistical significance, older animals tend to have higher latencies to enter the dark zone in both sessions, which could be attributed to general physiology and orientation aspects.

## DISCUSSION

We prepared $A\beta_{42}$ in different oligomeric states according to previously established protocols (O'Hare et al., 1999; Cameron et al., 2012; Cunvong et al., 2013; Nery et al., 2014) and analyzed their predominant nanoscale morphology and behavioral and cognitive effects after cerebroventricular injection in young and aged individuals. Considering the current perspective on the physiological and pathological contribution of these oligomeric states to AD, the clarification of structural characteristics of used preparations is of interest, as is their potential effects in differently aged adults.

Regarding the structural analysis using AFM, the distinct patterns observed in the three preparations confirm that we are working with different states of aggregation of $A\beta_{42}$ with morphological structures consistent with expectations for each form (Dahlgren et al., 2002a; Glabe, 2008). An apparent exception are the thin filaments seen in monomeric deposits. However, their small heights, often below 1 nm and short longitudinal repeat distances, suggest these structures are a line of monomers, most probably formed directly on the mica surface, as previously discussed. In addition, they are much different from the long, twisted, and entangled fibrillary arrays seen, e.g., in the protofibril preparation, or the globular structures that dominate oligomeric deposits. Comparison of the length of oligomers seen here to those reported in the literature for stabilized cross-linked oligomers of selected orders suggests the dominant order $n$ in our oligomer-enriched preparation to be 3–7 (Dahlgren et al., 2002b). However, the height of structures we see are small compared to $A\beta_{42}$ oligomers in early stages of aggregation adsorbed on graphene and measured in liquid (Nirmalraj et al., 2020). Furthermore, oligomer conformation is dynamic (Banerjee et al., 2017) and depict lateral sizes which are not very different among low order oligomers, making difficult identifying the class of oligomer based only on AFM size measurements. The most frequent diameter of fibrils found in our protofibrillar preparation (~4.5 nm) are compatible to sizes reported for the early stages of fibril formation (Nirmalraj et al., 2020), but yet they may appear intertwined in large fibril clusters. Of course, as $A\beta_{42}$ presents a complex aggregation dynamic, involving seeding and the formation of various oligomeric states in is path to the insoluble fibrillar form (Nirmalraj et al., 2020), there is obviously some structural heterogeneity in the preparations. Some degree of aggregation in the monomeric preparation in the form of small oligomers cannot be totally ruled out. Similarly, monomeric-like structures seem also to be present to a certain degree in the more aggregated preparations. But in general, their dominant morphological structures are clearly distinct.

Exploratory activity in a new tank to which animals were acclimated for 1 min was evaluated to ensure animals' exploratory capacity was preserved and their general physiology was uncompromised by the CV injection. Young and aged groups explored as expected relative to their body size. Larger bodied animals from the aged group were faster and travelled longer distances than young individuals. No significant effect of CV injection of $A\beta_{42}M$, $A\beta_{42}O$ or $A\beta_{42}P$ was observed in young individuals when compared to their respective control group (Fig. 3A–C). These results differ from work by (Bhattarai et al., 2016) that found a significant impairment of locomotory activity on animals of ages close to

young adults on the first 7 dpi. Javed et al. (2019) reported a change in swimming activity of 10-month-old zebrafish one week post injection. However, the concentration used was 50 μM, 5 times higher than ours. Bhattarai reported also slower swimming speed 3 days after injecting 20 μM of $A\beta_{42}$, a concentration also significantly higher than the one used here (Bhattarai et al., 2016). Aged animals showed more variation in their swimming performance on the Open Tank test, but only animals injected with $A\beta_{42}O$ had a significant reduction in distance travelled when compared to controls (Fig. 3E). Zebrafish swimming performance was reported to decrease with age by Gilbert et al. (2013), using a swim tunnel that forced fish to swim against a flow to maintain their position, which is more challenging than our general swimming observation.

When animals were tested at 21 dpi for long-term memory formation on the inhibitory avoidance, a similar pattern of effects was observed among young and aged individuals, suggesting that in the limited apparatus space, swimming performance effects were not impactful neither was their body size differences. Training latencies among all groups were equivalent, supporting these assumptions. Learning deficits were observed in young and aged animals injected with $A\beta_{42}O$ or $A\beta_{42}P$ (Fig. 4A, B), reinforcing the AOH perspective that larger soluble forms are deleterious. Our cognitive effects on the inhibitory avoidance are similar to what other groups have found (Bhattarai et al., 2016; Javed et al., 2019) using other behavioral tests.

The $A\beta_{42}O$ effect may result from a combination of cellular effects of oligomers such as overstimulation of extra synaptic NMDA receptors, leading to $Ca^{2+}$ upregulation, triggering a cascade of cytotoxic events leading to synaptic disruption and neuronal loss (Tu et al., 2014). The equivalent effects of the protofibrillar form may be attributed also to oligomeric parts shed by larger aggregates (Cohen et al., 2013) or by direct effects of protofibrils and fibrils on the neuronal vicinity. Interestingly, when injected with $A\beta_{42}M$ young and aged zebrafish demonstrated learning hability akin to control (veh) group, which is in agreement to demonstrations of monomers neuroprotective effects (Giuffrida et al., 2009) and other physiological roles extensively reviewed in (Brothers et al., 2018; Moir et al., 2018).

In this series of experiments, we focused on bringing together *in vivo* behavioral effects and *in vitro* characterization of $A\beta_{42}$ preparations and did not investigate the underlying mechanisms of the cognitive effects, which deserve attention and should be examined in following studies, including signaling and inflammatory responses caused by Aβ CV.

Taken together our behavioral effects are in accordance with current views on the positive and deleterious roles of the different oligomeric states of $A\beta_{42}$ on cognition. To be confident on our interpretation of the behavioral effects of their CV administration, it was critical to ensure that our preparations had the expected overall characteristics, confirmed by AFM. Amyloid aggregation is an active and complex process, in which any step in the aggregation process can give rise to a series of oligomeric species with varied size distribution and conformational properties and therefore analytical techniques must be applied accordingly. In addition to characterizing the different oligomeric presentations of $A\beta_{42}$ simultaneously, to ensure a proper comparison between all groups, we were especially attentive to the preparation and use of fresh Aβ solution. This is a critical methodological aspect, as findings may be masked by the dynamic changes in oligomeric forms that may occur spontaneously on Aβ solutions over time and may impede the comparison of results from different studies available on the literature until now.

While monomers tend to aggregate, protofibrillar and fibrillar forms are known to shed oligomeric parts in a process of secondary nucleation (Cohen et al., 2013), adding to the complexity of characterizing intermediary molecular structures of $A\beta_{42}$. Due to its dynamic equilibrium and complex balance in certain ranges of concentrations, it is difficult to affirm the real nature of the species observed on AFM as slight variation in protocols, solvents or substrates may also impact characterization. Importantly, the AFM analysis and their distinct effects on cognition support that our preparations are indeed enriched in the proposed $A\beta_{42}$ monomeric, oligomeric, and protofibrillar forms, despite the presence of occasional larger aggregates. A comparative analysis of the impact of solvents used for initial $A\beta_{42}$ solubilization on amyloid morphology and biological activity would be beneficial and the incorporation of additional characterization techniques could contribute to a better understanding of the intricate dynamics of amyloid aggregation.

An additional challenge is a varying terminology used to describe monomeric, protofibrillar or fibril forms in the literature. Our comprehensive approach aimed to contribute to this debate and our observations confirm that our three $A\beta_{42}$ preparations were structurally unique and within expected nanoscale dimensions and morphologies, in agreement with data presented by other research groups (Harper et al., 1997; Dahlgren et al., 2002a; Glabe, 2008; Nirmalraj et al., 2020). Our data reinforce new perspectives regarding $A\beta_{42}$ physiological and pathological roles that we plan to explore in the future.

## FUNDING

This study was supported by the Brazilian Federal Agency CNPq (425818/2018-7) and by the Coordenação de Aperfeiçoamento de Pessoal de Nível Superior – Brasil (CAPES) – Finance Code 001. M.V. and R.P. are a CNPq fellowship recipients P.P. and A. G. received CAPES fellowships.

We dedicate this to Ivan Izquierdo, great scientist and generous mentor.

## REFERENCES

Adamcik J, Jung J-M, Flakowski Jérôme, De Los Rios P, Dietler G, Mezzenga R (2010) Understanding amyloid aggregation by statistical analysis of atomic force microscopy images. Nat Nanotechnol 5(6):423–428.

Adamcik J, Mezzenga R (2012) Study of amyloid fibrils via atomic force microscopy. Curr Opin Colloid Interface Sci 17(6):369–376.
Altenhofen S, Wiprich MT, Nery LR, Leite CE, Vianna MRMR, Bonan CD (2017) Manganese(II) chloride alters behavioral and neurochemical parameters in larvae and adult zebrafish. Aquat Toxicol 182:172–183.
Banerjee S, Sun Z, Hayden EY, Teplow DB, Lyubchenko YL (2017) Nanoscale dynamics of amyloid β-42 oligomers as revealed by high-speed atomic force microscopy. ACS Nano 11 (12):12202–12209.
A. Baumketner Amyloid beta-protein monomer structure: A computational and experimental study Protein Science 15 3 420 428.
Benilova I, Karran E, De Strooper B (2012) The toxic Aβ oligomer and Alzheimer's disease: an emperor in need of clothes. Nat Neurosci 15(3):349–357.
Bhattarai P, Kuriakose A, Zhang Y, Kizil C (2017a) The effects of aging on Amyloid- b 42-induced neurodegeneration and regeneration in adult zebra fish brain. 4:1–8.
Bhattarai P, Thomas AK, Cosacak MI, Papadimitriou C, Mashkaryan V, Froc C, Reinhardt S, Kurth T, Dahl A, Zhang Y, Kizil C (2016) IL4/STAT6 signaling activates neural stem cell proliferation and neurogenesis upon amyloid-β42 aggregation in adult zebrafish brain. Cell Rep 17(4):941–948.
Bhattarai P, Thomas AK, Cosacak MI, Papadimitriou C, Mashkaryan V, Zhang Y, Kizil C (2017b) Modeling amyloid-β42 toxicity and neurodegeneration in adult zebrafish brain. J Vis Exp 2017:1–7.
Blank M, Guerim LD, Cordeiro RF, Vianna MRM (2009) Neurobiology of Learning and Memory A one-trial inhibitory avoidance task to zebrafish : Rapid acquisition of an NMDA-dependent long-term memory. Neurobiol Learn Mem 92:529–534 Available at: http://dx.doi.org/10.1016/j.nlm.2009.07.001.
Brothers HM, Gosztyla ML, Robinson SR (2018) The physiological roles of amyloid-β peptide hint at new ways to treat Alzheimer's disease. Front Aging Neurosci 10:1–16.
Cameron DJ, Galvin C, Alkam T, Sidhu H, Ellison J, Luna S, Ethell DW (2012) Alzheimer's-related peptide amyloid-?? plays a conserved role in angiogenesis. PLoS One 7:1–8.
Chen Y, Tang BL (2006) The amyloid precursor protein and postnatal neurogenesis/neuroregeneration. Biochem Biophys Res Commun 341(1):1–5.
Cline EN, Bicca MA, Viola KL, Klein WL (2018) The amyloid-β Oligomer hypothesis: beginning of the third decade. JAD 64(s1): S567–S610.
Cohen SIA, Linse S, Luheshi LM, Hellstrand E, White DA, Rajah L, Otzen DE, Vendruscolo M, Dobson CM, Knowles TPJ (2013) Proliferation of amyloid-β42 aggregates occurs through a secondary nucleation mechanism. Proc Natl Acad Sci U S A 110(24):9758–9763.
Cunvong K, Huffmire D, Ethell DW, Joshua Cameron D (2013) Amyloid-β increases capillary bed density in the adult zebrafish retina. Investig Ophthalmol Vis Sci 54:1516–1521.
Dahlgren KN, Manelli AM, Blaine Stine W, Baker LK, Krafft GA, Ladu MJ (2002a) Oligomeric and fibrillar species of amyloid-β peptides differentially affect neuronal viability. J Biol Chem 277:32046–32053 Available at: http://dx.doi.org/10.1074/jbc.M201750200.
Dahlgren KN, Manelli AM, Stine WB, Baker LK, Krafft GA, LaDu MJ (2002b) Oligomeric and fibrillar species of amyloid-β peptides differentially affect neuronal viability. J Biol Chem 277 (35):32046–32053.
Demuro A, Mina E, Kayed R, Milton SC, Parker I, Glabe CG (2005) Calcium dysregulation and membrane disruption as a ubiquitous neurotoxic mechanism of soluble amyloid oligomers. J Biol Chem 280(17):17294–17300.
Enache TA, Chiorcea-Paquim A-M, Oliveira-Brett AM (2016) Amyloid–β peptides time-dependent structural modifications: AFM and voltammetric characterization. Anal Chim Acta 926:36–47.
Giacomelli CE, Norde W (2005) Conformational changes of the amyloid β-peptide (1–40) adsorbed on solid surfaces. Macromol Biosci 5(5):401–407.
Gilbert MJH, Zerulla TC, Tierney KB (2013) Zebrafish (Danio rerio) as a model for the study of aging and exercise: Physical ability and trainability decrease with age. Experiment Gerontol 50:106–113.
Giuffrida ML, Caraci F, Pignataro B, Cataldo S, De Bona P, Bruno V, Molinaro G, Pappalardo G, Messina A, Palmigiano A, Garozzo D, Nicoletti F, Rizzarelli E, Copani A (2009) Beta-amyloid monomers are neuroprotective. J Neurosci 29(34):10582–10587.
Glabe CG (2008) Structural classification of toxic amyloid oligomers. J Biol Chem 283(44):29639–29643.
Hardy JA, Higgins GA (1992) Alzheimer's disease: the amyloid cascade hypothesis. Science (80-) 256:184–185.
Harper JD, Lieber CM, Lansbury PT (1997) Atomic force microscopic imaging of seeded fibril formation and fibril branching by the Alzheimer's disease amyloid-β protein. Chem Biol 4(12):951–959.
Hayes AJ, Reynolds S, Nowell MA, Meakin LB, Habicher J, Ledin J, Bashford A, Caterson B, Hammond CL, Heymann D (2013) Spinal deformity in aged zebrafish is accompanied by degenerative changes to their vertebrae that resemble osteoarthritis. PLoS One 8(9):e75787.
Heber S, Herms J, Gajic V, Hainfellner J, Aguzzi A, Rülicke T, Kretzschmar H, von Koch C, Sisodia S, Tremml P, Lipp H-P, Wolfer DP, Müller U (2000) Mice with combined gene knock-outs reveal essential and partially redundant functions of amyloid precursor protein family members. J Neurosci 20(21):7951–7963.
Hortschansky P, Schroeckh V, Christopeit T, Zandomeneghi G, Fändrich M (2005) The aggregation kinetics of Alzheimer's β-amyloid peptide is controlled by stochastic nucleation. Protein Sci 14(7):1753–1759.
Howe K et al (2013) The zebrafish reference genome sequence and its relationship to the human genome are involved in the ongoing improvement of the zebrafish genome assembly. Manual annotation was produced by G The generation of maps used in the initial assemblies and the pr. Nature 496(7446):498–503.
International Alzheimer's Disease (2019) World Alzheimer Report 2019.
Javed I, Peng G, Xing Y, Yu T, Zhao M, Kakinen A, Faridi A, Parish CL, Ding F, Davis TP, Ke PC, Lin S (2019) Inhibition of amyloid beta toxicity in zebrafish with a chaperone-gold nanoparticle dual strategy. Nat Commun 10(1).
Josephs KA, Whitwell JL, Ahmed Z, Maria M, Weigand SD, Knopman DS, Boeve BF, Parisi JE, Petersen RC, Dickson Jr DW, RJ, (2009) Beta-amyloid burden is not associated with rates of brain atrophy. Ann Neurol 63:204–212.
Kametani F, Hasegawa M (2018) Reconsideration of amyloid hypothesis and tau hypothesis in Alzheimer's disease. Front Neurosci 12 Available at: /pmc/articles/PMC5797629/ [Accessed October 4, 2021].
Li H, Liu CC, Zheng H, Huang TY (2018) Amyloid, tau, pathogen infection and antimicrobial protection in Alzheimer's disease - conformist, nonconformist, and realistic prospects for AD pathogenesis. Transl Neurodegener 7:1–16.
Lin YC, Komatsu H, Ma J, Axelsen PH, Fakhraai Z (2019) Identifying polymorphs of amyloid-β (1–40) fibrils using high-resolution atomic force microscopy. J Phys Chem B 123(49):10376–10383.
Livingston G et al (2017) Dementia prevention, intervention, and care. Lancet 390(10113):2673–2734.
Luo Y, Bolon B, Damore MA, Fitzpatrick D, Liu H, Zhang J, Yan Q, Vassar R, Citron M (2003) BACE1 (β-secretase) knockout mice do not acquire compensatory gene expression changes or develop neural lesions over time. Neurobiol Dis 14:81–88.
Matthews M, Varga ZM (2012) Anesthesia and Euthanasia in Zebrafish. ILAR J 53(2):192–204.
MCTIC (Ministério da Ciência, Tecnologia I e C (2016) Normativas do Concea – Lei, Decreto, Portarias, Resoluções Normativas e Orientações Técnicas, 3ª Edição. Available at: https://www.mctic.gov.br/mctic/export/sites/institucional/institucional/concea/arquivos/publicacoes/ebook-normativas.pdf.
Moir RD, Lathe R, Tanzi RE (2018) The antimicrobial protection hypothesis of Alzheimer's disease. Alzheimer's Dement 14:1602–1614. Available at: https://doi.org/10.1016/j.jalz.2018.06.3040.

Moores B, Drolle E, Attwood SJ, Simons J, Leonenko Z, Sokolov I (2011) Effect of surfaces on amyloid fibril formation. PLoS One 6 (10):e25954.

Nazem A, Mansoori GA (2008) Nanotechnology solutions for Alzheimer's disease: advances in research tools, diagnostic methods and therapeutic agents. JAD 13(2):199–223.

Nery LR oesler, Eltz NS ilva, Hackman C, Fonseca R, Altenhofen S, Guerra HN oriega, Freitas VM orais, Bonan CD enise, Vianna MR yff MR oca (2014) Brain intraventricular injection of amyloid-β in zebrafish embryo impairs cognition and increases tau phosphorylation, effects reversed by lithium. PLoS One 9: e105862.

Nery LR, Silva NE, Fonseca R, Vianna MRM (2017) Presenilin-1 targeted morpholino induces cognitive deficits, increased brain Aβ1−42 and decreased synaptic marker PSD-95 in zebrafish larvae. Neurochem Res 42(10):2959–2967.

Newman M, Ebrahimie E, Lardelli M (2014) Using the zebrafish model for Alzheimer's disease research. Frontiers Media SA. Available at: http://www.ncbi.nlm.nih.gov/pubmed/25071820 [Accessed August 14, 2016].

Cortes-Penfield NW, Trautner BW, RJ, (2016) Amyloid-β peptide protects against microbial infection in mouse and worm models of Alzheimer's disease. Sci Transl Med 8:139–148.

Nirmalraj PN, List J, Battacharya S, Howe G, Xu L, Thompson D, Mayer M (2020) Complete aggregation pathway of amyloid β (1–40) and (1–42) resolved on an atomically clean interface. Sci Adv 6(15).

Novo M, Freire S, Al-Soufi W (2018) Critical aggregation concentration for the formation of early Amyloid-β (1–42) oligomers. Sci Rep 8:3–10. Available at: http://dx.doi.org/10.1038/s41598-018-19961-3.

O'Hare E, Weldon DT, Manyth PW, Ghiraldi JR, Finke MP, Kuskowski MA, Maggio JE, Shephard RA, Cleary J (1999) Delayed behavioral effects following intrahippocampal injection of aggreated Aβ(1-42). Brain Res:1–10.

Parichy DM (2015) Advancing biology through a deeper understanding of zebrafish ecology and evolution Available at:. Elife 4:1–11. Available from: http://elifesciences.org/lookup/doi/10.7554/eLife.05635.

Pu YZ, Liang L, Fu AL, Liu Y, Sun L, Li Q, Wu D, Sun MJ, Zhang YG, Zhao BQ (2016) Generation of Alzheimer's disease transgenic Zebrafish expressing human APP mutation under control of Zebrafish appb promotor. Curr Alzheimer Res 14:668–679.

Ridley RM, Baker HF, Windle CP, Cummings RM (2006) Very long term studies of the seeding of β-amyloidosis in primates. J Neural Transm 113(9):1243–1251.

Sakono M, Zako T (2010) Amyloid oligomers: formation and toxicity of Aβ oligomers. FEBS J 277:1348–1358.

Saleem S, Kannan RR (2018) Zebrafish: an emerging real-time model system to study Alzheimer's disease and neurospecific drug discovery. Cell Death Discov 4(1).

Schneider LS, Mangialasche F, Andreasen N, Feldman H, Giacobini E, Jones R, Mantua V, Mecocci P, Pani L (2015) Disease: an appraisal from 1984 to 2014. 275:251–283.

Shankar GM, Li S, Mehta TH, Garcia-Munoz A, Shepardson NE, Smith I, Brett FM, Farrell MA, Rowan MJ, Lemere CA, Regan CM, Walsh DM, Sabatini BL, Selkoe DJ (2008) Amyloid β-protein dimers isolated directly from Alzheimer brains impair synaptic plasticity and memory. Nat Med 14:837. Available at: /pmc/articles/PMC2772133/ [Accessed October 4, 2021].

Singleman C, Holtzman NG (2014) Growth and Maturation in the Zebrafish, Danio Rerio: A staging tool for teaching and research. Zebrafish 11(4):396–406.

Stainier DYR, Raz E, Lawson ND, Ekker SC, Burdine RD, Eisen JS, Ingham PW, Schulte-Merker S, Yelon D, Weinstein BM, Mullins MC, Wilson SW, Ramakrishnan L, Amacher SL, Neuhauss SCF, Meng A, Mochizuki N, Panula P, Moens CB (2017) Guidelines for morpholino use in zebrafish. PLoS Genet 13.

Thomas PK et al (2017) Modeling amyloid-β42 toxicity and neurodegeneration in adult zebrafish brain. J Vis Exp 2017:1–7. Available at: https://pubmed.ncbi.nlm.nih.gov/29155703/ [Accessed October 4, 2021].

Tu S, Okamoto S, Lipton SA, Xu H (2014) Oligomeric A β -induced synaptic dysfunction in Alzheimer' s disease:1–12.

Washington PM, Morffy N, Parsadanian M, Zapple DN, Burns MP (2014) Experimental traumatic brain injury induces rapid aggregation and oligomerization of amyloid-beta in an Alzheimer's disease mouse model. J Neurotrauma 31 (1):125–134.

Watanabe-Nakayama T, Sahoo BR, Ramamoorthy A, Ono K (2020) High-speed atomic force microscopy reveals the structural dynamics of the amyloid-β and amylin aggregation pathways. Int J Mol Sci 21:1–30.

Westerfield M (2007) The zebrafish book: A guide for the laboratory use of zebrafish (Danio Rerio). Eugene: University of Oregon Press.

Wong K et al (2010) Analyzing habituation responses to novelty in zebrafish (Danio rerio). Behav Brain Res 208(2):450–457.

Yu L, Tucci V, Kishi S, Zhdanova IV (2006) Cognitive aging in zebrafish. PLoS One 1. Available at: https://journals.plos.org/plosone/article?id = 10.1371/journal.pone.0000014 [Accessed October 5, 2021].

*(Received 6 October 2021, Accepted 26 February 2022)*
*(Available online 08 March 2022)*